Supporting Information for

Nanostructure Impact on Electrocatalysis in Gold Nanodimers *via* Electrochemiluminescence Microscopy

Qian-Qian Tao, [a‡] Cong-Hui Xu, [b‡] Wei Zhao, [*b] Hong-Yuan Chen [a] and Jing-Juan Xu [a]

a State Key Laboratory of Analytical Chemistry for Life Science, School of Chemistry and Chemical Engineering, Nanjing University, Nanjing 210023, P.R. China
E-mail: xujj@nju.edu.cn

b Institute of Nanochemistry and Nanobiology, School of Environmental and Chemical Engineering, Shanghai University, Shanghai 200444, P.R. China
E-mail: wei_zhao@shu.edu.cn

‡ These authors contributed equally.

---------- Contents ----------

---

1. Experimental section.

Reagents and materials.

3-Aminopropyl triethoxysilane (APTES, 99%), Tris(2-carboxyethyl) phosphine (TCEP), Tripropylamine (TPrA, >99%) and Tris(2,2'-bipyridine) dichlororuthenium(II) hexahydrate ($Ru(bpy)_3Cl_2 \cdot 6H_2O$, 98%) were obtained from Sigma-Aldrich (U.S.A). Methoxymercapto polyethylene glycol (mPEG-SH) purchased from seebio (Shanghai, China). 8-Amino-5-chloro-7-phenylpyrido[3,4-d]-pyridazine-1,4[2H,3H]-dione (L-012, a luminol analogue) was bought from Wako Chemical U.S.A., Inc. (Richmond, VA). H_2O_2 (30%) were obtained from Sinopharm Chemical Reagent. 10X Phosphate buffered saline (PBS, pH 7.4) and 1 M Tris-HCl buffer solution (pH 8.0) was purchased from KeyGEN Biotech (Nanjing, China). Indium tin oxide (ITO)-coated glass slides (coating thickness, ~100 nm; resistance, ~10 Ω/square) were purchased from CSG (Shenzhen, China). Millipore water (Millipore, Inc., Bedford, MA) treated with 0.22 μm filter (PES membrane, Merck Millipore Ltd) was used throughout the experiments. The oligonucleotides were synthesized by Shanghai Sangon Biological Engineering Technology & Services Co. (Shanghai China). Detailed DNA sequences and modifications were shown in below.

Table S1. The DNA sequences.

Name	Sequences (5′- to -3′)
P30	SH-GTA ACG TCA ATG AGC AAA GGT ATT AAC TTT
S30	SH-AAA GTT AAT ACC TTT GCT CAT TGA CGT TAC
P24	SH-TGC AGT AGG TCA AGT ACG AGG TAA
S24	SH-TTA CCT CGT ACT TGA CCT ACT GCA
P15	SH-CGT AGG AGT CTG GAC
S15	SH-GTC CAG ACT CCT ACG
P9	SH-TGA GTC TCG
S9	SH-CGA GAC TCA

Apparatus for characterization.

The morphologies of Au NPs and Au NDs were characterized using JEOL200CX transmission electron microscopy (TEM) operated at 200kV. Scanning electron microscopy (SEM) images were acquired using a Hitachi S4800 (JEOL Ltd., Japan) operating at beam voltages of 5-15 KV. UV–vis adsorption spectroscopic characterization was performed using a Nanodrop-2000C spectrophotometer (Thermo Fisher Scientific Inc.). The film thickness was measured with a step meter (Bruker DektakXT). X-ray photoelectron spectroscopy (XPS) was collected from ESCALAB 250Xi (Thermo Scientific) with Al Kα X-ray radiation as X-ray source.

Synthesis of Au nanodimers (NDs) with varying interparticle distances.

Au NPs with a diameter of 80 nm were purchased from Ted Pella, Inc. The synthesis method of Au NDs was based on asymmetric modification and DNA hybridization according to previous literature.[1] Firstly, citrate-capped Au NPs were adsorbed onto amine group coated glass slides by electrostatic interactions and then modified asymmetrically with mPEG-SH. These PEGylated Au NPs were removed from glasses via ultrasonic treatment in 1.0 mL water for 5 min. Then, 100 μL of 1 μM thiolated DNA (P15 or S15) treated with TCEP for 1 h was added to 500 μL of asymmetrically modified Au NPs. Subsequently, 10 μL of 0.1 M NaCl was added to the above solution in five times and aged for 24 h with slow shaking. Next, NPs were resuspended in 500 μL

of Tris–HCl buffer after centrifugation to obtain the asymmetrically modified Au-P15 or Au-S15. At last, each 150 μL of Au-P15 and Au-S15 was hybridized and incubated at the temperature of 37 °C for 1 h. Au NDs with other gap distances were prepared by the above procedure using the corresponding DNA in place of P15 and S15. The formed Au NDs were preserved at 4 °C for following experiment.

Preparation of clean ITO and formation of aluminum layer on ITO.

ITO glasses were cleaned as previously reported by first boiled with a solution of isopropanol containing 2.0 M KOH for 15 min, followed by sonication with water, acetone, water, ethanol and water for 15 min.[2] Then the clean ITO was placed in an oven to dry at 100℃ for 1 h. An ultra-thin aluminum (Al) film was prepared on the surface of clean ITO via magnetron sputtering coating. The UV/ozone treatment for 30 min would efficiently to remove the organic components from the ITO slides in PSD-UV4 ozone system (Novascan Technologies). Subsequently, the Al film deposited under atmosphere pressure of 5×10^{-6} Pa by Kapoton Tape on the magnetron sputtering coating machine manufactured Kurt J. Lesker Trading Company Inc. (PVD75). Finally, it was stored in clean plastic plates and sealed.

Au NPs immobilization.

Clean ITO or ITO-Al slides were immersed in 1% APTES (ethanol) for 10 s and heated at 80 ℃ for 30 min. The obtained electrodes functionalized with $-NH_2$ were desired for the immobilization of nanoparticles. Au NPs with a suitable concentration (200 μL) suspended droplets was diluted on the aminated slide and electrostatic adsorbed for 1 h. The slide was then washed with distilled water three times to remove the unadsorbed Au NPs. Finally, electrodes with Au NPs was treated in PSD-UV4 ozone system UV for 30 min to remove ligands on the surface of the Au NPs and carry out the follow-up experiments.

Electrochemical and optical setup.

Dark-field microscopy was consisted of the inverted microscopy (IX73, Olympus), a dark-field condenser ($0.8 < NA < 0.92$) and a 60X objective lens (NA 0.75). Olympus true-color digital camera DP80 were used to capture dark-field image and the scattering spectrum was obtained with a monochromator (Acton SP2358, PI, USA) (grating density: 300 lines/mm; blazed wavelength: 500 nm) combined with liquid nitrogen cooled PyLoN CCD cameras (Princeton Instruments (PI), USA). The ECL microscopy setup was based on DFM. A digital delay/pulse generator triggered synchronously the electron multiplying CCD (EMCCD, Andor iXon Ultra 888) and electrochemical workstation (CHI600E, Chenhua Shanghai). The ECL imaging was operated in a shielding room. ITO with Au nanocatalysts immobilized on its surface was used as working electrode. A platinum wire (0.5 mm diameter) electrode and an Ag/AgCl wire electrode were immersed into the pool as the counter electrode and the reference electrode respectively. Double potential step chronoamperometry with suitable time interval was adopted as the applied potential. A circular hole shaped electrochemical reaction cell was prepared with polydimethylsiloxane (PDMS). For the ECL imaging, 5 mM luminophore (L-012 or $Ru(bpy)_3^{2+}$) and 50 mM coreactant (H_2O_2 or TPrA) were freshly prepared before every experiment. ECL images were acquired at potential of 0.55 V and 1.20 V, respectively. The exposure time was 2 s for L-012 and 5 s for $Ru(bpy)_3^{2+}$.

Finite Difference Time Domain simulation.

The Finite Difference Time Domain (FDTD) simulations were carried out to perform the extinction spectra and electric field intensities of Au monomer and dimers with variable gap distance.[3] The distance between two Au NPs was set from 2 nm to 10 nm with water as the medium environment, which the refractive index of surrounding medium was set as 1.33. A total-field scattered-field (TFSF) source with circular polarization by averaging over two orthogonal polarizations simulated the ECL emission light. The light source height was set to 100 nm. All of the mesh step during this simulation was 1 nm. The refractive index data of Gold were obtained from the built-in database of the software (Au (gold) – John and Christy).

Calculation of photon counts.

The A/D (analog-to-digital) counts of the camera is described below.

$$A/D\ counts = \frac{N_p \times QE \times EM\ Gain}{A/D\ unit} \#\ (1)$$

where N_p is the number of photons (photon counts) incident to the pixel, QE is the photoelectric conversion efficiency (94% in this case), $EM\ Gain$ is the electron multiplication coefficient of the camera, and $A/D\ unit$ is the analog-to-digital conversion coefficient which is 4.91 for the EMCCD we used in the experiment. The $EM\ Gain$ selected in the experiment is 300. And the background signals have been subtracted for statistical analysis.

Calculation of the heterogeneous electron transfer rate constant at Au NPs and Au NDs-modified electrodes.

To compare the reaction rates on dimers and monomers, we conducted ensemble electrochemical experiments to determine the heterogeneous electron-transfer rate constant ($\boldsymbol{k^0}$). For these measurements, we synthesized Au NDs, and deposited equal mass of Au NDs and Au NPs onto glassy carbon electrodes (GCE) for the ensemble analysis. Cyclic voltammetry (CV) was performed on electrodes modified with Au NDs and Au NPs at varying scan rates in a 5 mM $Ru(bpy)_3^{2+}$ solution, the $\boldsymbol{k^0}$ at Au NPs and Au NDs-modified electrodes was determined using Nicholson equation.[4, 5]

$$\boldsymbol{k}^0 = \psi \left[\frac{\pi DnFv}{RT}\right]^{\frac{1}{2}} \quad (2)$$

$$\psi = (-0.6288 + 0.0021X/(1 - 0.017X) \quad (3)$$

$$X = \Delta E_p \times n \quad (4)$$

where ψ is dimensionless rate parameter in CV. The potential difference between the anodic and cathodic peaks in CV is used to determine the dimensionless rate parameter ψ across a range of scan rates. D is the diffusion coefficient (1×10^{-5} cm^2 s^{-1}), n is the number of electrons, F is Faraday's constant (96,485 C mol^{-1}), v is the scan rate in CV (V s^{-1}), R is gas constant (8.314 J mol^{-1} K), and T is the temperature (298.15 K). At different scan rate, ΔE_p and ψ was calculated and shown in **Table S2** to **Table S6**. And k^0 were extracted from the slope of the fitting lines according to Nicholson equation in **Fig S8.**

Table S2. Peak separation, ΔE_p, parameter ψ used to calculated $\boldsymbol{k^0}$ of Au NPs at different scan rate with 5 mM $Ru(bpy)_3^{2+}$.

Scan rate (V/s)	ΔE_p (mV)	ψ
0.025	73.6	1.888
0.05	76.3	1.577
0.075	79.2	1.335
0.1	80.6	1.241
0.125	82.8	1.116
0.15	83.8	1.066
0.175	85.0	1.012
0.2	86.4	0.954

Table S3. Peak separation, ΔE_p, parameter ψ used to calculated $\boldsymbol{k^0}$ of Au NDs with interparticle distances of 3 nm at different scan rate with 5 mM $Ru(bpy)_3^{2+}$.

Scan rate (V/s)	ΔE_p (mV)	ψ
0.025	65.8	4.137
0.05	67.5	3.302
0.075	69.9	2.560
0.1	71.2	2.278
0.125	72.8	2.003
0.15	74.4	1.785
0.175	77.2	1.494
0.2	79.5	1.314

Table S4. Peak separation, ΔE_p, parameter ψ used to calculated $\boldsymbol{k^0}$ of Au NDs with interparticle distances of 5 nm at different scan rate with 5 mM $Ru(bpy)_3^{2+}$.

Scan rate (V/s)	ΔE_p (mV)	ψ
0.025	66.1	3.961
0.05	68.9	2.826
0.075	70.6	2.400
0.1	72.5	2.050
0.125	74.1	1.822
0.15	75.3	1.680
0.175	76.4	1.567
0.2	78.5	1.387

Table S5. Peak separation, ΔE_p, parameter ψ used to calculated $\boldsymbol{k^0}$ of Au NDs with interparticle distances of 8 nm at different scan rate with 5 mM $Ru(bpy)_3^{2+}$.

Scan rate (V/s)	ΔE_p (mV)	ψ
0.025	66.2	3.906
0.05	69.4	2.687
0.075	71.6	2.203
0.1	73.5	1.902
0.125	75.3	1.680
0.15	77.2	1.494
0.175	77.7	1.451
0.2	79.0	1.350

Table S6. Peak separation, ΔE_p, parameter ψ used to calculated $\boldsymbol{k^0}$ of Au NDs with interparticle distances of 10 nm at different scan rate with 5 mM $Ru(bpy)_3^{2+}$.

Scan rate (V/s)	ΔE_p (mV)	ψ
0.025	66.4	3.800
0.05	69.0	2.797
0.075	71.2	2.278
0.1	73.3	1.930
0.125	74.7	1.749
0.15	76.2	1.587
0.175	77.4	1.476
0.2	79.6	1.307

2. COMSOL simulation.

COMSOL Multiphysics 6.2a was employed to determine concentration profiles of Ru (III) ion species with three-dimensional finite element modeling.

Table S7. Reactions and parameters.

Electrochemical redox reactions	E^0(V) vs. Ag/AgCl	k_0(cm/s)
(1)$Ru(bpy)_3^{3+} + e^- \xrightarrow{k_1} Ru(bpy)_3^{2+}$	1.06	0.02
(2)$TPrA^{\cdot+} + e^- \xrightarrow{k_2} TPrA$	0.90	0.6
(3) $P + e^- \xrightarrow{k_3} TPrA^{\cdot}$	≤1.7	\

Homogeneous Reactions	k_f
(4) $TPrA^{\cdot+} \rightarrow TPrA^{\cdot} + H^+$	537(s^{-1})
(5) $HA \rightarrow H^+ + A^-$	6.3×10^{-8}($M^{-1}s^{-1}$)
(6) $TPrA + HA \rightarrow A^- + TPrAH$	6.3×10^{-9}($M^{-1}s^{-1}$)
(7) $Ru(bpy)_3^{2+} + TPrA^{\cdot} \rightarrow Ru(bpy)_3^{3+} + P$	10^{10}($M^{-1}s^{-1}$)
(8) $Ru(bpy)_3^{+} + Ru(bpy)_3^{3+} \rightarrow Ru(bpy)_3^{2+*} + Ru(bpy)_3^{2+}$	10^{10}($M^{-1}s^{-1}$)
(9) $Ru(bpy)_3^{3+} + TPrA \rightarrow TPrA^{\cdot+} + Ru(bpy)_3^{2+*}$	1 ($M^{-1}s^{-1}$)
(10) $Ru(bpy)_3^{3+} + TPrA^{\cdot} \rightarrow Ru(bpy)_3^{2+*} + P$	10^{10}($M^{-1}s^{-1}$)
(11) $Ru(bpy)_3^{+} + TPrA^{\cdot+} \rightarrow Ru(bpy)_3^{2+*} + TPrA$	10^{6}($M^{-1}s^{-1}$)
(12) $Ru(bpy)_3^{2+*} \rightarrow Ru(bpy)_3^{2+} + hv$	15848(s^{-1})

Notes: (P stands for TPrA loses two electrons and one proton. HA means H_2PO_4. All the parameters are from the previous literature.[6])

Reactions 1, 2, 4, 7, 8 and 12 were considered in numerical simulation. In this simulation, all redox and intermediate species are assumed to have no adsorption onto the nanoplates, their mass transfer coefficients remain the same as those in bulk solution near the particles. The initial concentration of $Ru(bpy)_3^{2+}$ and TPrA are 5 mM and 50 mM respectively. Other parameters for simulations: R=8.31 J/(K·mol)，T=298 K，F=96485 C/mol，f = F/RT=38.92 V^{-1}.

Table S8. Variables used in digital simulation.

Chemical	Expression	Unit
$Ru(bpy)_3^{2+}$	$\frac{\partial Ru(II)}{\partial t} = D\nabla^2 C_{Ru(II)} - k_7\times Ru(II)\times TPrA + k_8\times Ru(I)\times Ru(III) + Ru^*\times k_{12}$	mol/(m^3.s)
$Ru(bpy)_3^{3+}$	$\frac{\partial Ru(III)}{\partial t} = D\nabla^2 C_{Ru(III)} - k_8\times Ru(I)\times Ru(III)$	mol/(m^3.s)
$Ru(bpy)_3^{+}$	$\frac{\partial Ru(I)}{\partial t} = D\nabla^2 C_{Ru(I)} + k_7\times Ru(II)\times TPrA - k_8\times Ru(I)\times Ru(III)$	mol/(m^3.s)
$Ru(bpy)_3^{2+*}$	$\frac{\partial Ru*}{\partial t} = D\nabla^2 C_{Ru*} + k_8\times Ru(I)\times Ru(III) - Ru^*\times k_{12}$	mol/(m^3.s)
TPrA	$\frac{\partial TPrA}{\partial t} = D\nabla^2 C_{TPrA}$	mol/(m^3.s)
$TPrA^{\cdot+}$	$\frac{\partial TPrA.+}{\partial t} = D\nabla^2 C_{TPrA.+} - k_4\times TPrA^{\cdot+}$	mol/(m^3.s)
$TPrA^{\cdot}$	$\frac{\partial TPrA.}{\partial t} = D\nabla^2 C_{TPrA.} + k_4\times TPrA^{\cdot+} - k_7\times Ru(II)\times TPrA^{\cdot}$	mol/(m^3.s)

3. Characterizations of Au NPs and Au NDs.

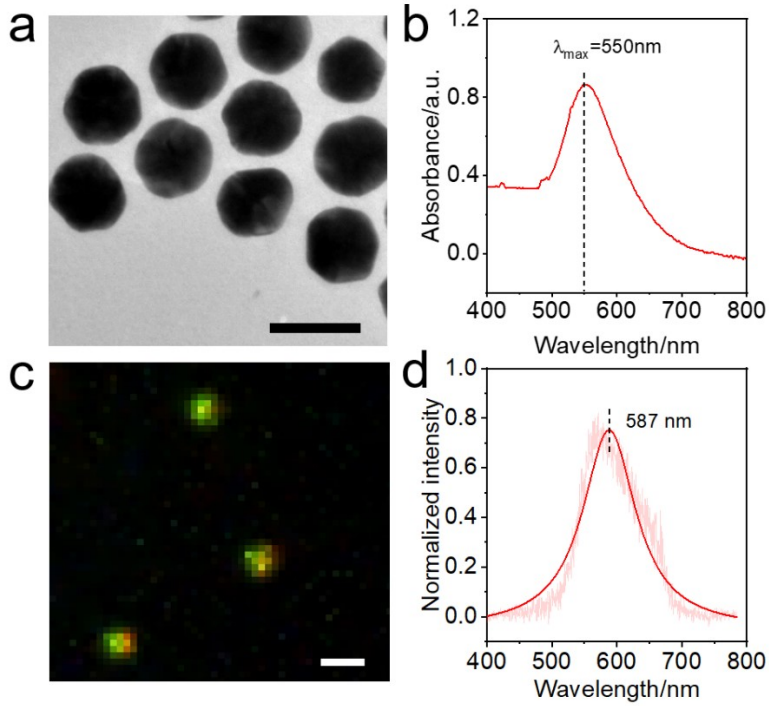

Fig. S1 (a) TEM and (b) absorption spectrum of Au NPs with a diameter of 80 nm. Scale bar: 100 nm. (c) DFM image of Au NPs and (d) corresponding LSPR scattering spectrum after Lorentz fitting of a single Au NP.

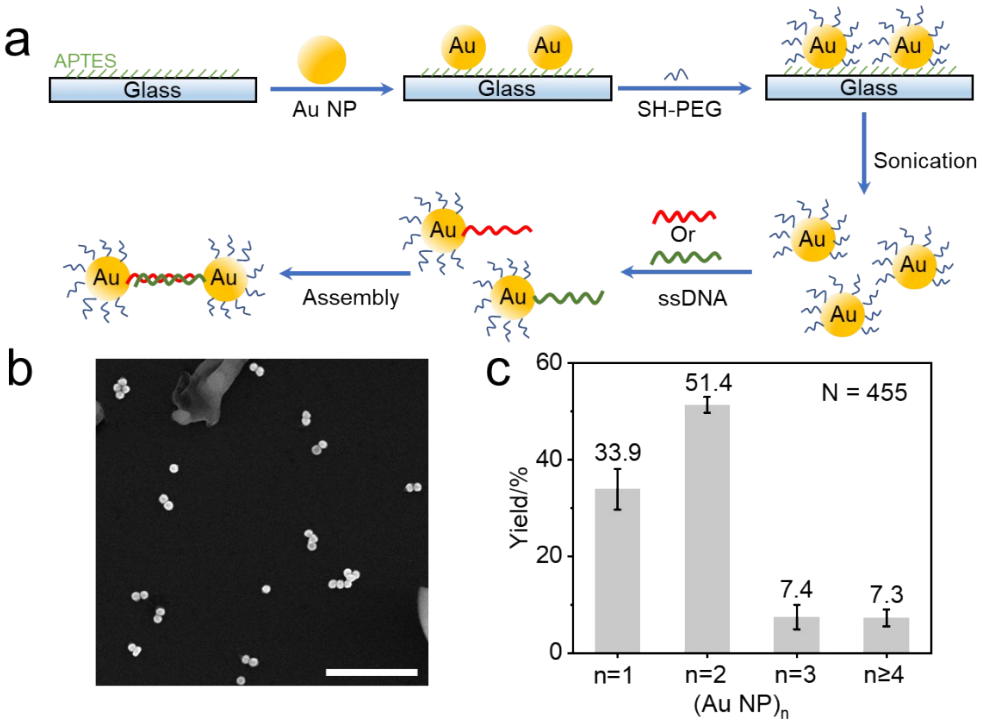

Fig. S2 (a) Scheme for stepwise DNA-mediated Au NDs assembly using asymmetric modification. (b) SEM image of Au NDs and (c) population distribution of the particles by DNA-mediated assembly; 51.4% of the 455 total particles correspond to dimers. Scale bar: 1 μm.

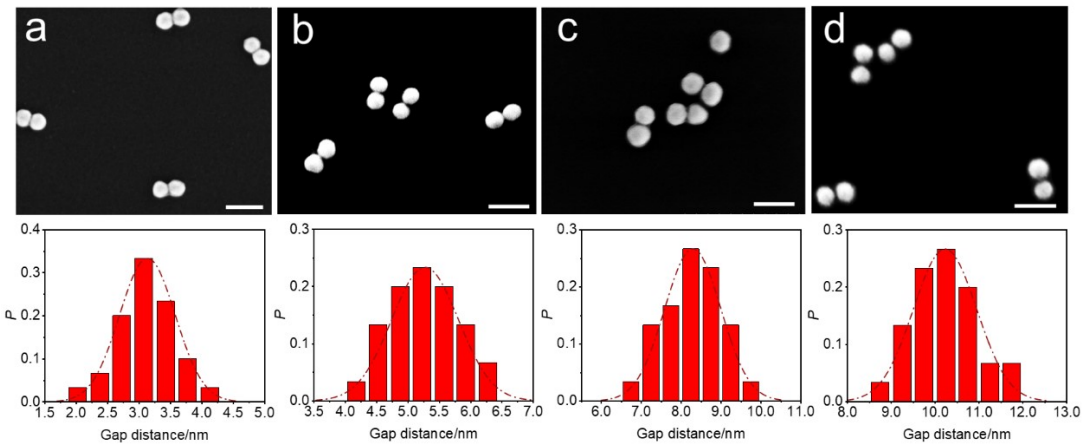

Fig. S3 (a-d) Morphological characterization of Au NDs with varying interparticle distances by SEM. Scale bar: 200 nm. Bottom: corresponding gap distance histograms.

4. Simulation of extinction and scattering spectra of Au NDs.

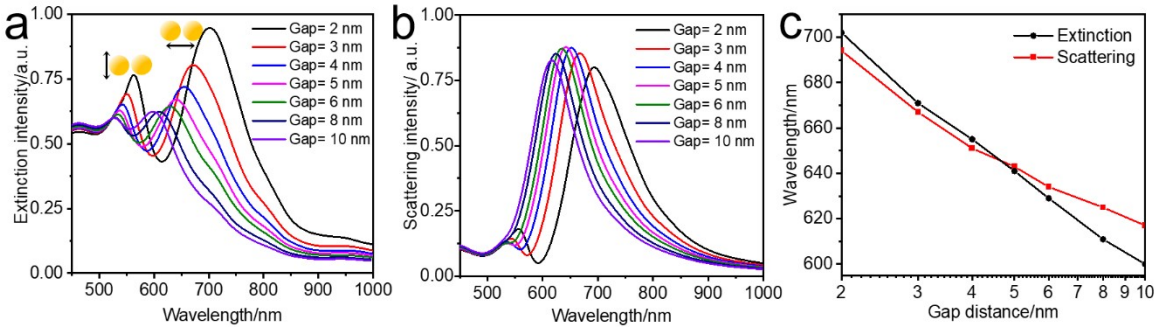

Fig. S4 (a) Simulated extinction spectra and (b) scattering spectra of a nanosphere dimer as a function of gap distance. (c) Plot of intense extinction wavelength and maximum scattering wavelength of Au NDs.

5. Characterization of Al layer on ITO.

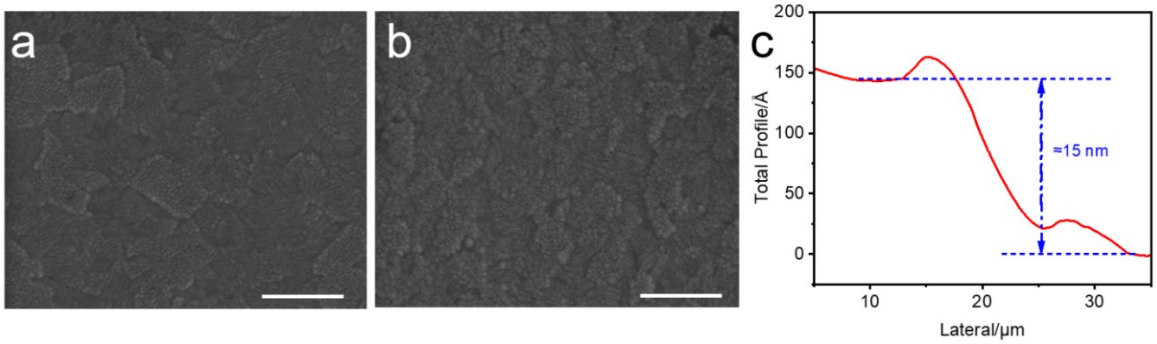

Fig. S5 SEM images of (a) ITO and (b) ITO-Al. Scale bar: 500 nm. (c) Thickness of thin Al film on ITO substrate measured by step meter.

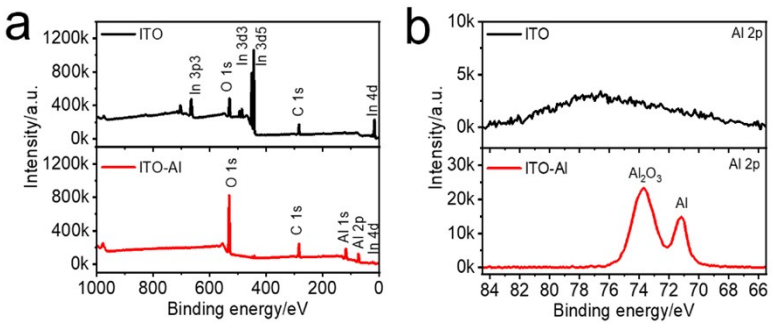

Fig. S6 (a) X-ray photoemission spectroscopy (XPS) spectrum of ITO substrate and ITO-Al. And (b) Al 2p peak of ITO and ITO-Al.

6. Gaussian fitting of single emitting spots.

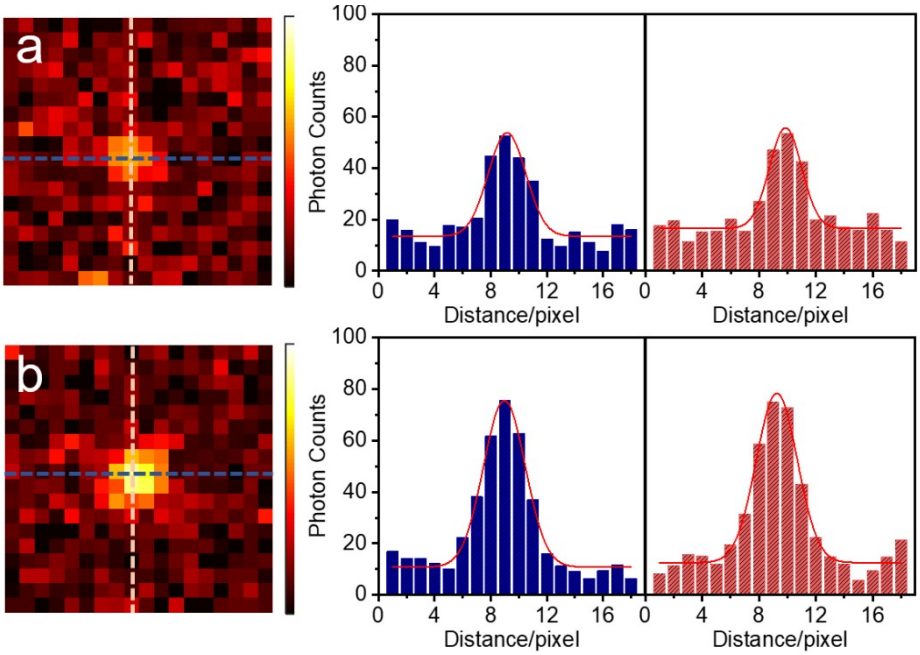

Fig. S7 ECL emission of single (a) Au NP and (b) Au ND, and corresponding photon counts profile along with the horizontal (blue) and vertical (orange) lines.

7. The heterogeneous electron transfer rate constant at Au NPs and Au NDs-modified electrodes.

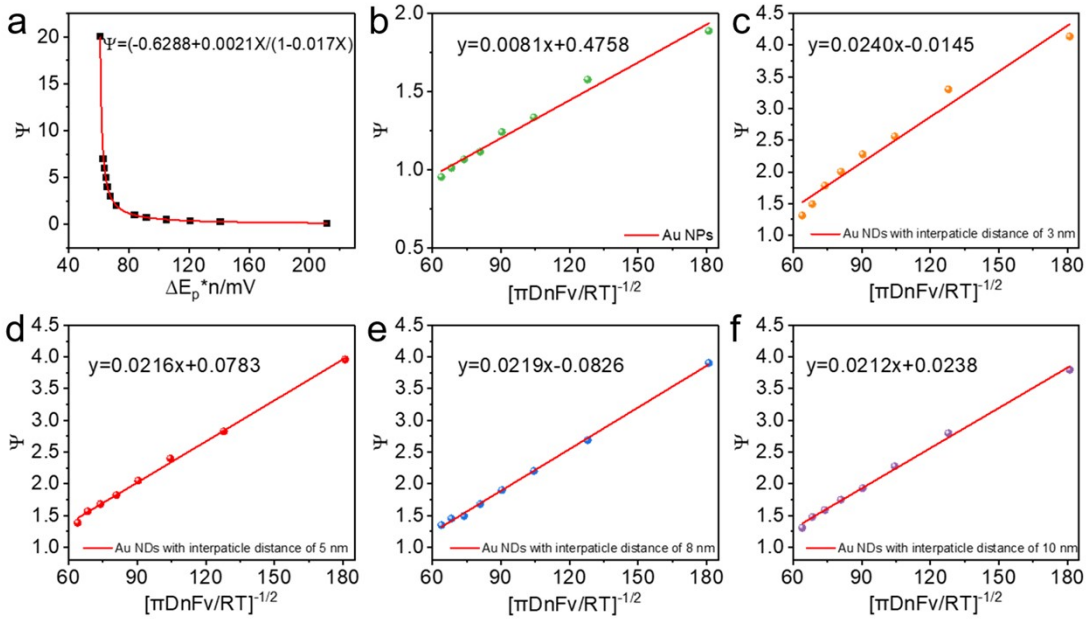

Fig. S8 (a) Plot of theoretical (square symbols) ψ *vs.* ΔE_p according to Nicholson's method: the solid line represents the fitting curve. (b-f) plots of ψ *vs.* $[\pi DnFv/(RT)]^{-1/2}$ for Au NPs and Au NDs with interparticle distance of 3 nm, 5 nm, 8 nm and 10 nm. $\boldsymbol{k^0}$ were extracted from the slope of the fitting lines according to Nicholson equation.

Table S9. The calculated heterogeneous electron transfer rate constant ($\boldsymbol{k^0}$).

	$\boldsymbol{k^0}$ ($cm \cdot s^{-1}$)
Au NPs	0.0081
Au NDs with interparticle distance of 3 nm	0.0240
Au NDs with interparticle distance of 5 nm	0.0216
Au NDs with interparticle distance of 8 nm	0.0219
Au NDs with interparticle distance of 10 nm	0.0212

8. Digital simulation results of Au NDs.

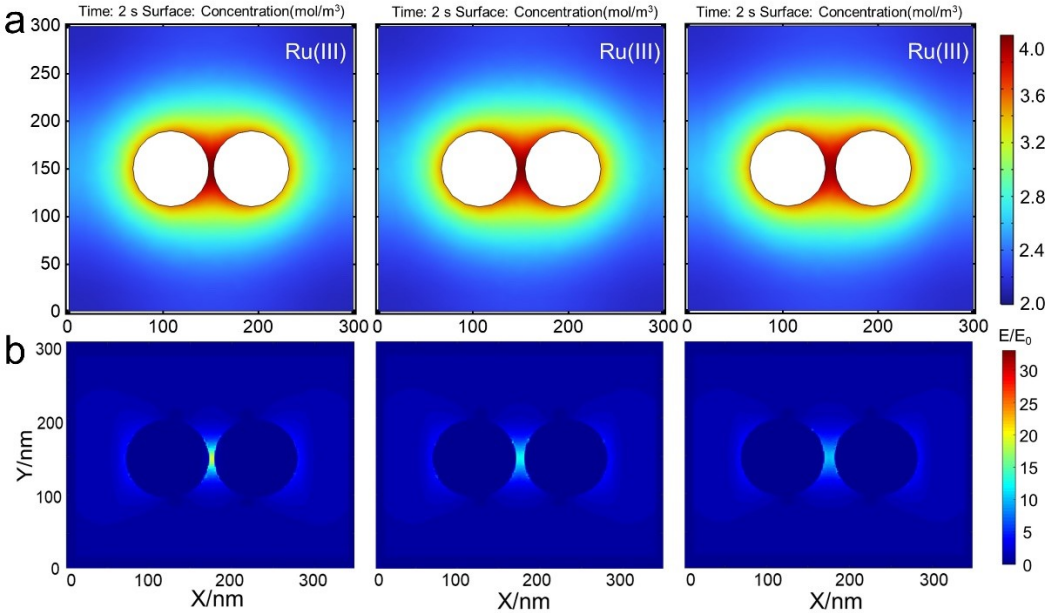

Fig. S9 (a) The simulated Ru(III) concentration gradient and (b) EM field distribution around Au NDs with interparticle distances of 5 nm, 8 nm and 10 nm.

9. ECL of trimers and tetramer.

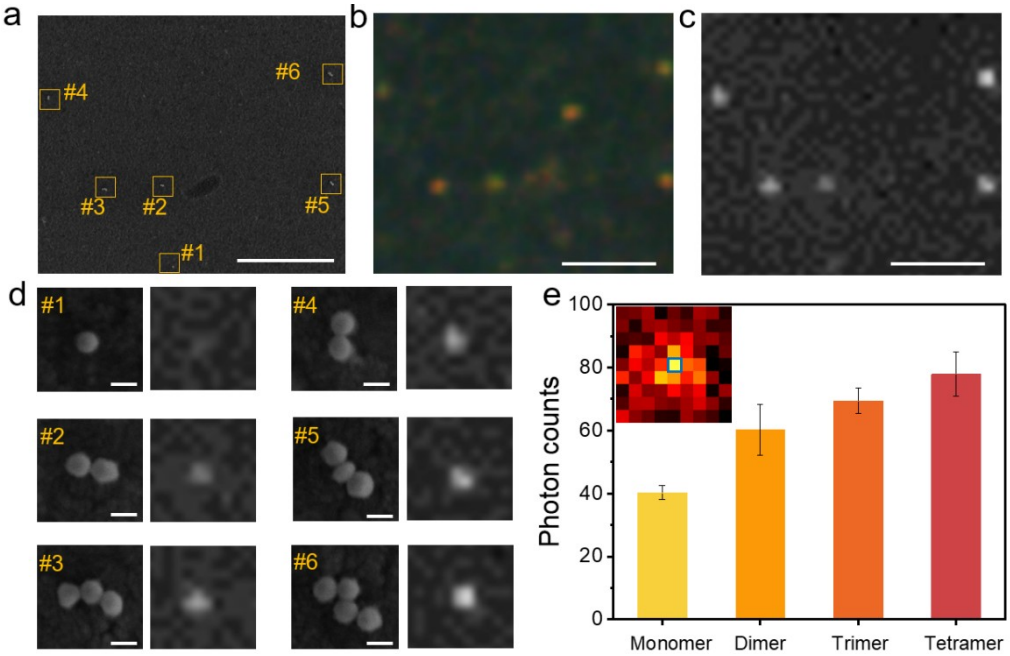

Fig. S10 (a) SEM, (b) Dark-field microscopy and (c) corresponding ECL microscopy images of single Au NP (monomer) and NP aggregates (dimer, trimer and tetramer) using L-012 as the luminophore. Scale bar: 5μm. Each particle in the SEM was indexed by numbers in yellow. (d) High-resolution SEM image, ECL image and ECL photon counts of each particle in the area. Scale bar: 100 nm. (e) The ECL photon counts at the central pixel for monomers, dimers, trimers and tetramers.

10. References

1. X. L. Li, Z. L. Zhang, W. Zhao, X. H. Xia, J. J. Xu and H. Y. Chen, *Chem. Sci.*, 2016, **7**, 3256-3263.

2. M. J. Zhu, J. B. Pan, Z. Q. Wu, X. Y. Gao, W. Zhao, X. H. Xia, J. J. Xu and H. Y. Chen, *Angew Chem. Int. Ed.*, 2018, **57**, 4010-4014.

3. M. X. Li, W. Zhao, G. S. Qian, Q. M. Feng, J. J. Xu and H. Y. Chen, *Chem. Commun.*, 2016, **52**, 14230-14233.

4. R. S. Nicholson, *Anal. Chem.*, 1965, **37**, 1351–1355.

5. I. Lavagnini, R. Antiochia and F. Magno, *Electroanalysis*, 2004, **16**, 505-506.

6. T. C. Lee, M. Alarcón-Correa, C. Miksch, K. Hahn, J. G. Gibbs and P. Fischer, *Nano Lett.*, 2014, **14**, 2407-2412.